# Nanoscale

Accepted Manuscript


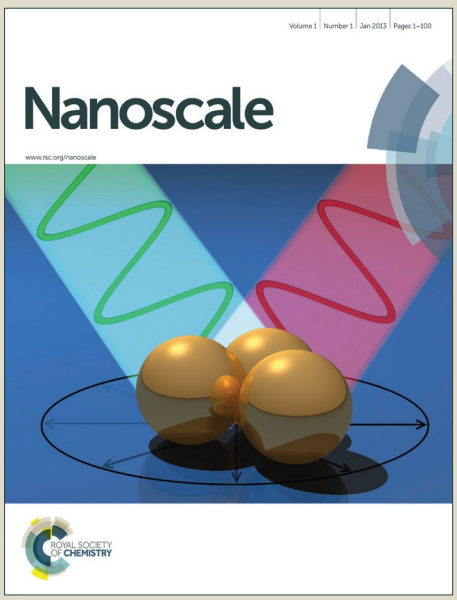





ROYAL SOCIETY OF CHEMISTRY

www.rsc.org/nanoscale

Nanoscale

RSCPublishing

ARTICLE

# Tuning nonlinear optical absorption properties of $WS_2$ nanosheets

Cite this: DOI: 10.1039/x0xx00000x

Hui Long[#], Lili Tao[#], Chun Yin Tang, Bo Zhou, Yuda Zhao, Longhui Zeng, Siu Fung Yu , Shu Ping Lau, Yang Chai, and Yuen Hong Tsang*

Received 00th June 2015,
Accepted 00th July 2015

DOI: 10.1039/x0xx00000x

www.rsc.org/

To control the optical properties of two-dimensional (2D) materials is a long-standing goal, being of both fundamental and technological significance. Tuning nonlinear optical absorption (NOA) properties of 2D transition metal dichalcogenides in a cost effective way has emerged as an important research topic because of its possibility to costume design NOA properties, implying enormous applications including optical computer, communications, bioimaging, and so on. In this study, $WS_2$ with different size and thickness distribution was fabricated. Results demonstrate that both NOA onset threshold, $F_{ON}$, and optical limiting threshold, $F_{OL}$, of $WS_2$ under the excitation of nanosecond pulsed laser can be tuned over a wide range by controlling its size and thickness. The $F_{ON}$ and $F_{OL}$ show a rapid decline with the decrease of size and thickness. Due to the edge and quantum confinement effect, $WS_2$ quantum dots (2.35 nm) exhibit the lowest $F_{ON}$ (0.01 J/cm$^2$) and $F_{OL}$ (0.062 J/cm$^2$) among all the samples, which are comparable to the lowest threshold achieved in the graphene based materials, showing great potential as NOA materials with tunable properties.

## Introduction

Graphene, the earliest discovered two-dimensional (2D) material, has become well known for its excellent electrical, optical, magnetic, mechanical properties, and so on.[1-3] However, it remains a challenge to tune its electronic and optical properties because opening or engineering the zero-bandgap structure of graphene usually involve complicated processes to break the lattice symmetry.[4,5] As a kind of newly emerging 2D layered materials, transition metal dichalcogenides (TMDs) are different from zero-bandgap graphene, offering a wide range of intrinsic open bandgap structure and properties by changing different combination of transition metal groups and chalcogen. The dependence of bandgap structure of TMDs on the thickness results in its thickness-tunable bandgap properties, as well as tunable optical, electrical and electrochemical property, arousing considerable interest among researchers around the world because of their wide applications including solar cells, photodetectors, transistors, water splitting, and so on.[6-12]

$WS_2$ is a typical TMD material with large layer distance, making it easier to be separated from the bulk to few-layer through various physical and chemical methods. In this research, ultrasonic exfoliation method was used because of its simplicity and scalability. When $WS_2$ is thinned from bulk to single layer, its bandgap changes from 1.3 eV indirect to 2.1 eV direct bandgap structure.[13] And the resulting enhancement of UV-Vis absorption has significant implications for solar cell, photodetector, photocatalysis, and other optical applications.[10,11] Moreover, these bandgap changes will improve the transition probability from the valance band to the conduction band of the material, leading to the enhancement of the nonlinear optical absorption (NOA) such as two photon absorption (TPA).[14]

Being able to control the nonlinear optical properties of nanoscale materials is one of the most fundamental manipulations of light for the development of micro-photonics.[15] Therefore, a cost effective method to tune the nonlinear optical properties of the nanoscale TMDs have attracted enormous research interest due to its wide potential applications including optical limiting, bioimaging, optical communication, optical computer, data storage, drug delivery, and photodynamic therapy. [16-18]

In this study, $WS_2$ flakes were exfoliated by an ultrasonic technique followed by a gradient centrifugation separation as shown in Fig. S1. In brief, 0.05 g $WS_2$ powder was dispersed in 50 ml N-methyl-pyrrolidone (NMP) and treated with ultrasonic for 15 h at a power of 400 W. A simple gradient centrifugation was then employed to select the size and thickness of $WS_2$ in a certain range. Subsequently, the $WS_2$ sheets were incorporated in Polymethylmethacrylate (PMMA) to form a solid composite for the NOA studies. The detail of this fabrication method is discussed in the experimental section.

## Experimental Section

**Chemicals:** Tungsten sulfide ($WS_2$) powder (~6 μm, 99.99%), N-methyl-2-pyrrolidone (NMP) (>99.0%), Methyl methacrylate (MMA) (99.0%), Benzoyl peroxide (BPO) (≥96.0%) were all purchased from Aladdin in Shanghai, China.

### Preparation of $WS_2$/PMMA and $WS_2$ QD/PMMA bulk:

$WS_2$ nanosheets and quantum dots are first prepared through an ultrasonic exfoliation method followed by a gradient centrifugation

process as shown in Fig. S1. In detail, 0.05 g $WS_2$ powder was dispersed in 50 ml NMP and treated with ultrasonic for 15 h at a power of 400 W. The obtained exfoliated $WS_2$ sheets dispersion was then centrifuged at a successive rate, ω, equal to 10000, 7000, 5000, 1000 and 500 rpm for 30 min, respectively. The concentrations of all these five dispersions were adjusted to the same 0.087 mg/ml. Then, solid state $WS_2$/PMMA composites were fabricated, 20 ml MMA and 2 ml $WS_2$ sheets or quantum dots dispersions were first mixed and heated at 75°C for 10 mins, and then 0.023 g BPO was added and heated again at 75 °C for another 10 mins, followed by another heat treatment at 105 °C for 20 min. Finally, they were kept at 75 °C for 30 hours and solid transparent $WS_2$/PMMA samples were obtained. The digital images of the composites are presented in Fig. 2S. Composites turn from colorless to bright yellow with smaller and thinner $WS_2$ flakes embedded.

**Characterization:**

The size and thickness distribution of $WS_2$ sheets and quantum dots were given based on the images obtained by the atomic force microscope (AFM, Veeco Nanoscope V) in tap mode. The UV-Vis-NIR absorption spectra were recorded in the wavelength range of 400-1100 nm using a scanning spectrophotometer (Shimadzu) at room temperature. The morphology of $WS_2$ QDs was investigated using a field emission transmission electron microscope (FETEM, JEOL Model JEM-2100F). The nonlinear optical absorption properties were examined by open aperture Z-scan method using a 8 ns pulsed Nd:YAG Laser (Quanta-Ray GCR-168) operating at a repetition of 10Hz with pulse energy of ~2000 μJ corresponding to the laser intensity of 8.9 GW/cm$^2$ and 28 GW/cm$^2$ at the laser focal point for 532 and 1064 nm, respectively.

## Results and Discussion

Fig. 1 (a-d) show the atomic force microscopy (AFM) images of the

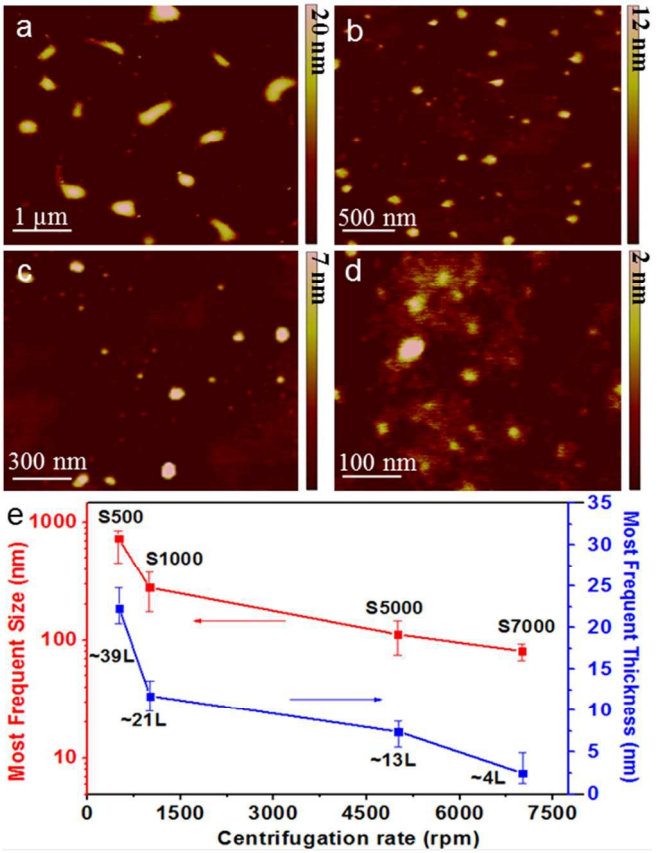


**Fig. 1** (a-d) AFM images of $WS_2$ sheets exfoliated in NMP and subsequently separated under different centrifugation rates of 500, 1000, 5000, and 7000 rpm, respectively. For each $WS_2$ sample, about 50 sites were sampled for size and thickness analysis. (e) Most frequent size and thickness of the four samples, L - Estimated layer number.

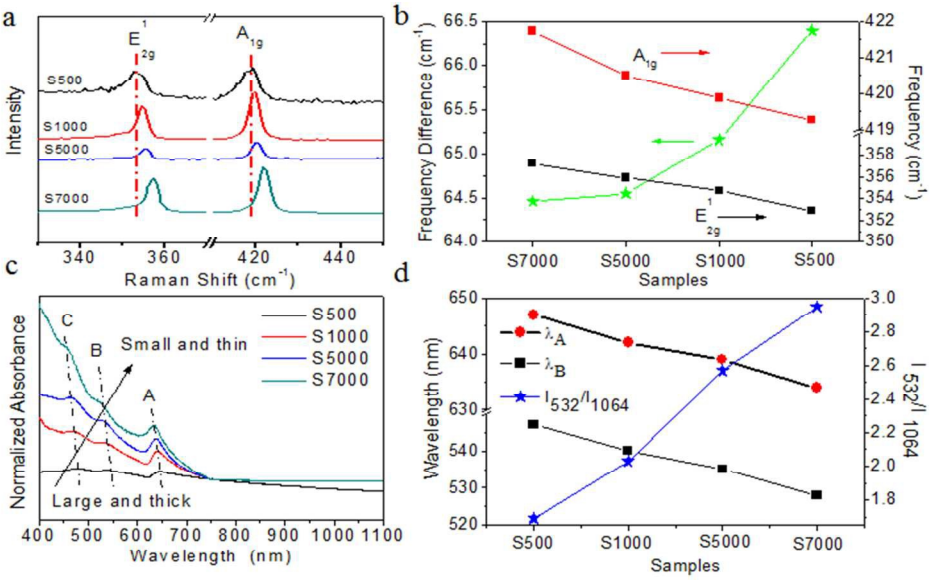


**Fig. 2** (a) Raman spectra. (b) The peak frequency of $E^1_{2g}$, $A_{1g}$ and their frequency difference . (c) Absorption spectra. (d) Peak positions of the characteristic peaks A and B, and ratios of absorption intensity at 532 nm to 1064 nm ($I_{532}/I_{1064}$) of $WS_2$ suspension in NMP selected at 500 rpm, 1000 rpm, 5000 rpm and 7000 rpm centrifugation rate, respectively.

$WS_2$ sheets obtained after 15 hours of ultrasonic exfoliation and subsequent centrifugation at 500, 1000, 5000, 7000 rpm, which were named after S500, S1000, S5000 and S7000 samples, respectively. With the increasing centrifugation rate, smaller and thinner $WS_2$ sheets can be obtained (Fig. S3-5), which has also been confirmed by K. G. Zhou *et al*.,[19] and smaller $WS_2$ sheets would be beneficial for the TPA process. [20] The most frequent size and thickness of the four samples are presented in Fig. 1e. The most frequent size decreases from about 1 to 0.1μm and the most frequent thickness decreases from about 24.1 nm to 2.6 nm for the samples from S500 to S7000. The quantified changes agree well with the AFM images shown in Fig. 1 (a-d). From the thickness distributions shown in Fig. S4, it is confirmed that $WS_2$ sheets with different thickness (layer number) ranges can be separated effectively through the simple ultrasonic exfoliation and centrifugation method.

The Raman spectra and normalized UV-Vis-NIR absorption spectra of $WS_2$ sheets suspensions in NMP collected at different centrifugation rates were measured and given in Fig. 2. Two characteristic Raman peaks, $E^1_{2g}$ and $A_{1g}$ of $WS_2$ are observed in Fig. 2a. $E^1_{2g}$ is hardened with the decreasing layer number, which is due to increasing long range Coulombic interaction of the in-plane vibrations of Mo atoms, resulting in the blue shift of $E^1_{2g}$ peak, as shown in Fig. 2a and 2b.[21] $A_{1g}$ mode is related to the out-of-plane vibration of S atoms which is also hardened and shows a blue shift with the decreasing layer number as presented in Fig. 2a and 2b. The blue shift of the $A_{1g}$ peak with decreasing layer number is different from the previous reported ones.[22,23] This phenomenon may be explained by the size effect. With the decreasing size of $WS_2$ sheets, the momentum conservation will be relaxed and the Raman active modes will not be limited to be at the center of the Brillouin zone, causing the blue shift of $A_{1g}$ peak which has been reported in the $TiO_2$ nanoparticles and Si nanosolid.[24,25] Fig. 2c presents the absorption intensity in the UV-Vis range showing a significant increase for the smaller and thinner $WS_2$ sheets collected at higher centrifugation rate, consequently making it closer to direct bandgap semiconductor with stronger bandgap absorption. The two characteristic excitonic absorption peaks A and B of $WS_2$ are observed along with a higher energy density of states peak C. The excitonic absorption peaks A and B are due to the direct transition from the valance band to the conduction band involving a spin-orbit split valence band at the K point of the Brillouin zone.[26] With increasing centrifugation rate, all the three peaks show blue shifts, being consistent with the results reported by Coleman et al.[27] As presented in Fig. 2d, the peak wavelength of A and B bands gives a similar decline tendency ($\lambda_A$ and $\lambda_B$) with the increase of collecting centrifugation rate for obtaining smaller and thinner $WS_2$. Such behavior was observed in other TMDs, such as $MoS_2$ and $WSe_2$.[28,29] The ratios of absorption intensity at 532 nm to 1064 nm is also plotted in Fig. 2b, showing a considerable $I_{532/1064}$ change with a two fold increase from S500 to S7000. This result indicates the relative absorption at 532 nm is stronger than that at 1064 nm for smaller and thinner $WS_2$ sheets.

A standard open aperture Z-scan apparatus was used to measure the NOA properties of $WS_2$ incorporated in PMMA. All experiments were performed by using a 8-ns Nd:YAG pulsed Q-switched laser operating at a repetition of 10 Hz. The beam was focused using a 5 cm focal length lens. Schematic diagram of the experimental setup is shown in Fig. S6. The output fluence ($F_{out}$) was measured with respect to various input fluence ($F_{in}$) created by moving the sample along the z-direction around the focus. Fig. 3 presents the NOA performance of the $WS_2$/PMMA composite samples. At both 532 and 1064 nm, the output fluence shows a linear dependence on input fluence for the pure PMMA contrast to its nonlinear dependence after $WS_2$ sheets are embedded, indicating the matrix PMMA has no contribution to the NOA property of $WS_2$/PMMA. Fig. 3a and 3b present plots of $F_{out}$ versus $F_{in}$ for the $WS_2$/PMMA composites at 532 and 1064 nm, respectively. The ratio $F_{out}/F_{in}$ in the limit of zero fluence gives the linear transmittance ($T_L$)

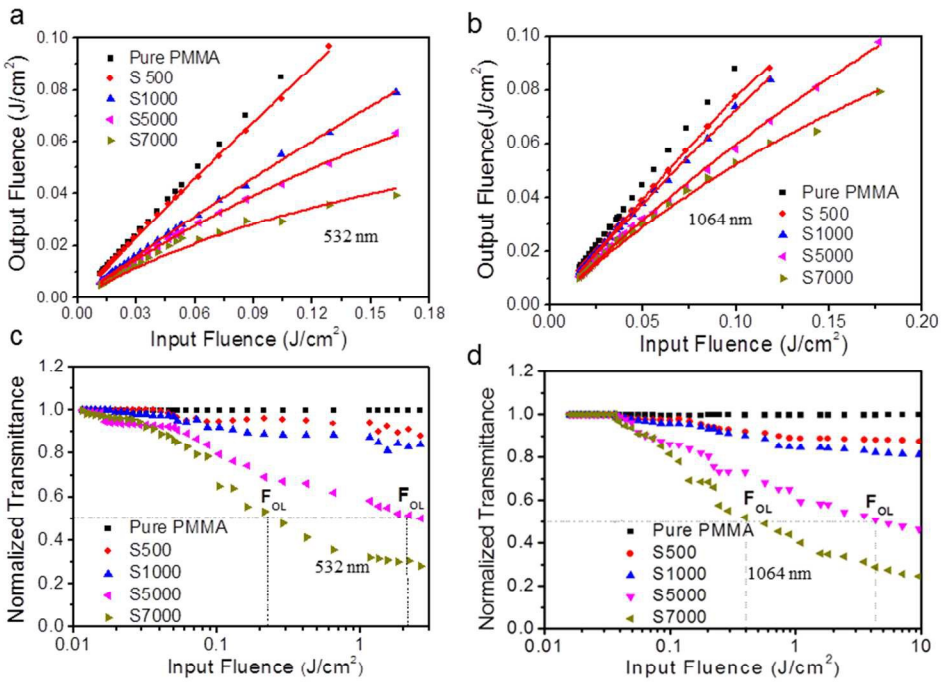


**Fig. 3** Nonlinear optical absorption performance of $WS_2$/PMMA composites. (a) and (b) are the output influence dependence on input fluence, the red lines are the fitting curve according to the TPA model. (c) and d) are the corresponding normalized transmittance dependence on the input fluence at 532 nm and 1064 nm, respectively.

All $WS_2$/PMMA composites exhibit a gradually reduced transmission with increasing incident energy for both wavelengths 532 and 1064 nm, indicating clearly a broad NOA response. Here, only the nonlinear optical reverse saturable absorption (RSA) property of $WS_2$ is observed but not saturable absorption (SA) reported by others.[20] It is believed that the pumping laser intensity of these experiments is too high to observe the SA phenomenon of $WS_2$ occurred under lower pumping intensity.[30,31] Fig. 3c and 3d show the variation of normalized transmittance as a function of the input fluence for different $WS_2$/PMMA samples under excitation wavelengths of 532 and 1064 nm, respectively. The NOA onset threshold ($F_{ON}$) is defined as the input fluence at which the normalized transmittance begins to deviate from linearity, and the optical limiting threshold ($F_{OL}$) is defined as the input fluence at which the normalized transmittance dropped to 50%. The values of $F_{ON}$ and $F_{OL}$ obtained from Fig. 3 are presented in Table 1. As two-photon absorption (TPA) is considered as the major mechanism for the optical limiting effect of $WS_2$,[32,33] the TPA coefficient (β) are also obtained by fitting the NOA data according to the TPA model and shown in Table 1.[14] The $T_L$, $F_{ON}$, $F_{OL}$ show a remarkable decrease with decreasing the size and thickness, indicating that smaller size and fewer layers of $WS_2$ sheets hold more sensitive NOA property with greater two-photon absorption (TPA) coefficient β. However, when comparing the sample S5000 to S7000, the most frequent size only dropped slightly 28% but the most frequent thickness reduced in 67% that lead to significant drops in $F_{ON}$ and $F_{OL}$ by 31% and 91%, respectively. These results indicate that the thickness plays a key role in tuning the NOA property. Sample S7000 exhibits excellent nonlinear optical property at both wavelengths of 532 and 1064 nm. For instance, the values of $F_{ON}$ and $F_{OL}$ at 532 nm are measured to be 0.011 $J \cdot cm^{-2}$ and 0.245 $J \cdot cm^{-2}$, respectively. These thresholds are close to the 2D single-layer graphene embedded polycarbonate (PC) matrix,[34] and much lower than other existent nonlinear optical materials including metal nanostructures,[35,36] carbon nanotubes,[35] graphene oxide,[37,38] graphene nanosheet and nanoribbon.[39] (See Table S1 in supporting information).

The improved NOA property for the smaller and thinner $WS_2$ sheets can be attributed to the following two possible reasons. On the one hand, with the thickness of $WS_2$ sheet being reduced from around tens of layers (S500) to few layers (S7000), its bandgap structure gradually changes from indirect to direct due to an interlayer interaction, thus greatly enhancing the transition probability from the valence band to conduction band and resulting in the enhanced absorption. Also, with considerable quantum-confinement effect, smaller size will lead to stronger absorption. This has been observed in $MoS_2$ as well.[40] Therefore, the absorption coefficient of $WS_2$ is enhanced greatly as shown in Table S2. And the enhanced absorption of the thin layer $WS_2$ can benefit TPA at both wavelengths of 532 and 1064 nm. With the highest absorption coefficient of sample S7000, the transition probability of photon from the valence band to conduction band would also be the highest, resulting in the best NOA performance. Moreover, the ratio $I_{532}/I_{1064}$ of S7000 is about twice that of S500, indicating the potential enhancement of the NOA property. On the other hand, with the smallest size of $WS_2$ sheets, sample S7000 has the largest surface area to volume ratio and more exposed free active edges, which also benefit to the TPA process.[27]

It has been shown that a higher ultrasonic power for a long time could allow the preparation of TMDs QDs by a direct liquid exfoliation. [41] In this study, the $WS_2$ QDs are successively obtained by ultrasonic $WS_2$ flakes in NMP for 15 hours but with a much higher centrifugation rate up to 10000 rpm. Fig. 4a shows the transmission electron microscopy (TEM) images of the $WS_2$ QDs together with the size distribution of the $WS_2$ QDs shown in inset. It is clearly observed that the obtained $WS_2$ QDs is quite small and uniform with the most frequent diameter and standard deviation of 2.35 nm and 0.03 nm, respectively. This agrees well with the HRTEM image of several typical $WS_2$ QDs (Fig. 4b). As presented in Fig. 4c, a single $WS_2$ QD of diameter 3.12 nm with an in-plane lattice spacing of 0.27 nm matches well with the (100) planes, in which the lattice fringes of the $WS_2$ QDs is also clearly observed. The corresponding selected area Fast Fourier Transform (FFT) image is shown in Fig. S7c, revealing the hexagonal crystalline structure. Fig. 4d gives the topography image of $WS_2$ QDs with the height profiles of the two randomly selected $WS_2$ QDs labeled as 1 and 2 shown in Fig. 4e. The average height of these $WS_2$ QDs is about 2.7 nm, corresponding to a few (~4) atomic layers of $WS_2$ QDs. The height distribution of the $WS_2$ QDs obtained from the AFM image is shown in Fig. 4f, indicating most of the $WS_2$ QDs are

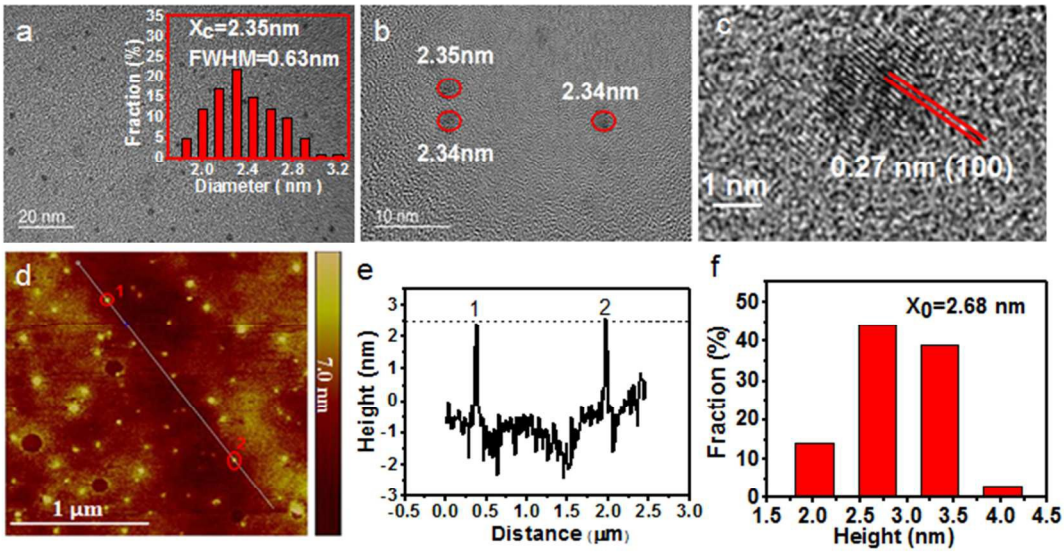


**Fig. 4** (a)TEM image, Inset: Size distribution of $WS_2$QDs (b, c) HRTEM images, and (d) AFM topography image of $WS_2$ QDs. (e) height profile of the section marked in (d). (f) Height distribution of the $WS_2$ QDs.



 

Table 1. Optical parameters of linear transmittance ($T_L$), two-photon absorption (TPA) coefficient (β), NOA onset thresholds ($F_{ON}$) and optical limiting thresholds ($F_{OL}$) for various $WS_2$/PMMA composites.

| Samples | 532 nm | | | | 1064 nm | | | |
|---|---|---|---|---|---|---|---|---|
| | $T_L$(%) | β (cm/GW) | $F_{ON}$ (J/cm$^2$) | $F_{OL}$ (J/cm$^2$) | $T_L$(%) | β (cm/GW) | $F_{ON}$ (J/cm$^2$) | $F_{OL}$(J/cm$^2$) |
| S500 | 79 | 3.91 | 0.035 | — | 80 | 2.29 | 0.05 | — |
| S1000 | 54 | 6.52 | 0.026 | — | 78 | 6.26 | 0.044 | — |
| S5000 | 52 | 21.51 | 0.016 | 2.6 | 67 | 11.35 | 0.039 | 4.32 |
| S7000 | 44 | 44.46 | 0.011 | 0.245 | 65 | 21.87 | 0.036 | 0.48 |
| $WS_2$QDs | 48 | 156.5 | 0.01 | 0.062 | 63 | 75.8 | 0.03 | 0.1 |

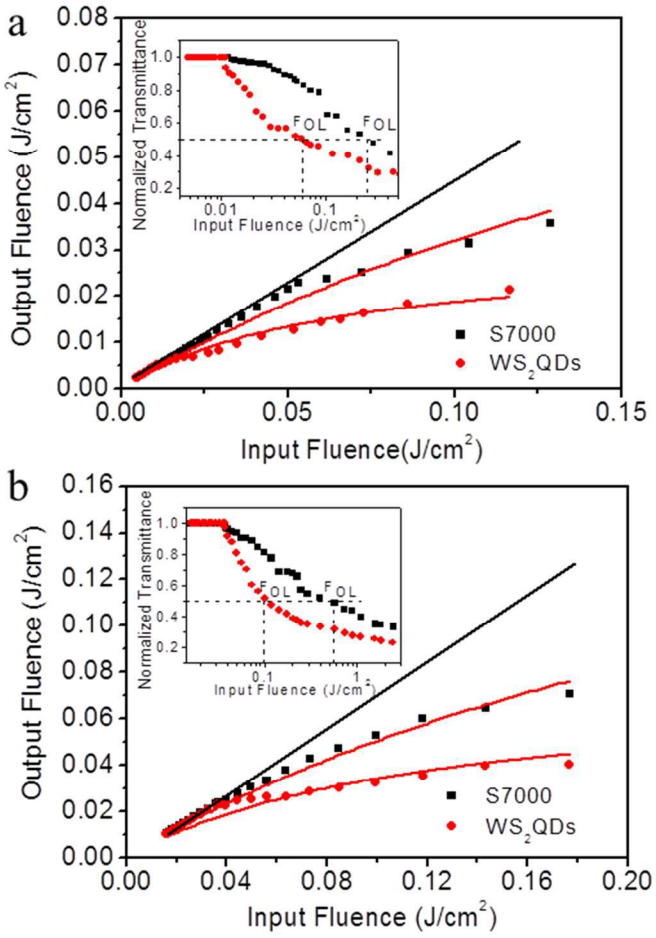


**Fig. 5** The comparison of NOA response of S7000 and $WS_2$ QDs at (a) 532 nm and (b) 1064 nm, respectively. Insets are the corresponding normalized transmittance dependence on the input fluence.

of 4 or 5 layers. From the data statistics, $WS_2$ QDs have the similar diameter and height due to the random orientation, then it can be regarded as sphere.

These fabricated $WS_2$ QDs are also incorporated in PMMA for NOA response measurement, and the results are shown in Fig. 5. Compared with S7000, $WS_2$ QDs exhibits much lower $F_{ON}$ and $F_{OL}$ at 532 nm and 1064 nm as shown in Table 1. These threshold values are comparable to the lowest demonstrated record of single-layer graphene which is considered as one of the best NOA materials,[34] and lower than all the demonstrated records of the traditional metal nanoparticles, carbon nanotube, graphene oxide (Table S1). We attribute the excellent NOA performance of $WS_2$ QDs to the edge and quantum confinement effects. Assuming the $WS_2$ sheet of S7000 as cylinder and QDs as sphere, the active surface area to volume ratio of $WS_2$ QDs is about 25 times higher than that of sample S7000. Therefore, $WS_2$ QDs has much more active surface and edges. The active edges of $WS_2$ lead to sub-bandgap absorption and further enhance the NOA performance,[42] SA or RSA, depending on the value of the laser input fluence.[30,31] Moreover, $WS_2$ QDs has stronger quantum confinement effect because of their ultrasmall size. Active edges and quantum confinement effect can further enhance NOA behavior due to the enhanced two-photon and three-photon absorption, which is a commonly acknowledged theory.[43,44]

## Conclusions

In summary, the $WS_2$ sheets in different size and thickness ranges and ultrasmall $WS_2$ QDs have been successfully fabricated using simple and effective liquid phase exfoliation technique. The NOA property of $WS_2$ sheet incorporated in PMMA show a close dependence on both size and thickness, and it has been confirmed that the smaller and thinner $WS_2$ contributes to a remarkably enhanced NOA performance (lower $F_{ON}$ and $F_{OL}$). The widely tunable NOA properties have been achieved through a control of size and thickness. More significantly, the NOA performance exhibited in $WS_2$ QDs is comparable to the best result of graphene based materials reported so far, having very low $F_{ON}$ (0.01 J/cm$^2$, 0.03 J/cm$^2$) and $F_{OL}$ (0.062 J/cm$^2$, 0.1 J/cm$^2$) at 532 nm and 1064 nm respectively, which is attributed to the edge and quantum confinement effects.

## Acknowledgements

This work is financially supported by the Research Grants Council of Hong Kong, China (Project Number: GRF 526511/PolyU B-Q26E), and the Hong Kong Polytechnic university (Project Number: G-YBB5, 1-ZE14).

## Notes and references

Department of Applied Physics and Materials Research Center, The Hong Kong Polytechnic University, Hung Hom, Kowloon, Hong Kong.
Email address: yuen.tsang@polyu.edu.hk
# These authors contributed equally to this work.

1 R. R. Nair, M. Sepioni, I.L. Tsai, O. Lehtinen, J. Keinonen, A. V. Krasheninnikov, T. Thomson, A. K. Geim, I. V. Grigorieva, *Nat. Phys.*, 2012, **8**, 199.

2 M. Liu, X. Yin, E. Ulin-Avila, B. Geng, T. Zentgraf, L. Ju, F. Wang, X. Zhang, *Nature.,* 2011, **474**, 64.
3 Y. Zhao, Z. Liu, T. Sun, L. Zhang, W. Jie, X. Wang, Y. Xie, Y. H. Tsang, H. Long, Y. Chai, *ACS Nano.,* 2014, **8**, 12601.
4 F. Bonaccorso, Z. Sun, T. Hasan, A. C. Ferrari, *Nat. Photonics.,* 2010, **4,** 611.
5 F. Yavari, C. Kritzinger, C. Gaire, L. Song, H. Gulapalli, T. Borca-Tasciuc, P. M. Ajayan, N. Koratkar, *Small.,* 2010, **6**, 2535.
6 B. Radisavljevic, A. Radenovic, J. Brivio, V. Giacometti, A. Kis, *Nat. Nanotechnol.,* 2011, **6**, 147.
7 W. Wu, L. Wang, Y. Li, F. Zhang, L. Lin, S. Niu, D. Chenet, X. Zhang, Y. Hao, T. F. Heinz, *Nature.,* 2014, **514**, 470.
8 Q. H. Wang, K. Kalantar-Zadeh, A. Kis, J. N. Coleman, M. S. Strano, *Nat. Nanotechnol.,* 2012, **7**, 699.
9 T. Georgiou, R. Jalil, B. D. Belle, L. Britnell, R. V Gorbachev, S. V Morozov, Y.-J. Kim, A. Gholinia, S. J. Haigh, O. Makarovsky, *Nat. Nanotechnol.,* 2013, **8**, 100.
10 D. Voiry, H. Yamaguchi, J. Li, R. Silva, D. C. B. Alves, T. Fujita, M. Chen, T. Asefa, V. B. Shenoy, G. Eda, *Nat. Mater.,* 2013, **12**, 850.
11 X. Hong, J. Kim, S.F. Shi, Y. Zhang, C. Jin, Y. Sun, S. Tongay, J. Wu, Y. Zhang, F. Wang, *Nat. Nanotechnol.,* 2014, **9**, 682.
12 K. Wang, J. Wang, J. Fan, M. Lotya, A. O'Neil, D. Fox, Y. Feng, X. Zhang, B. Jiang, Q. Zhao, H. Zhang, J. N. Coleman, L. Zhang and W. Blau, *ACS Nano*., 2013, **7**, 9260.
13 A. L. Elías, N. Perea-López, A. Castro-Beltrán, A. Berkdemir, R. Lv, S. Feng, A. D. Long, T. Hayashi, Y. A. Kim, M. Endo, *ACS Nano.,* 2013, **7**, 5235.
14 L. Tao, H. Long, B. Zhou, S. F. Yu, S. P. Lau, Y. Chai, K. H. Fung, Y. H. Tsang, J. Yao, D. Xu, *Nanoscale.,* 2014, **6**, 9713.
15 L. W. Tutt, T. F. Boggess, *Prog. Quant. Electr.,* 1993, **17**, 299.
16 L. Cao, X. Wang, M. J. Meziani, F. Lu, H. Wang, P. G. Luo, Y. Lin, B. A. Harruff, L. M. Veca, D. Murray, S. Xie, Y. Sun, *J. Am. Chem. Soc.,* 2007, **129**, 11318.
17 M. O. Senge, M. Fazekas, E. G. A. Notaras, W. J. Blau, M. Zawadzka, O. B. Locos, E. M. N. Mhuircheartaigh, *Adv. Mater. ,* 2007, **19**, 2737.
18 G. Zhou, W. Y. Wong, S. Y. Poon, C. Ye, Z. Lin, *Adv. Funct. Mater.,* 2009, **19**, 531.
19 K.-G. Zhou, M. Zhao, M.-J. Chang, Q. Wang, X.-Z. Wu, Y. Song, and H.-L. Zhang, *Small.*, 2015, **11**, 694.
20 K. Wang, Y. Feng, C. Chang, J. Zhan, C. Wang, Q. Zhao, J. N. Coleman, L. Zhang, W. J. Blau, and J. Wang, *Nanoscale.*, 2014, **6**, 10530.
21 B. Chakraborty, H. S. S. Ramakrishna, A. K. Sood and C. N. R. Rao. J. *Raman Spectrosc*., 2013, **44**, 92.
22 H. Zeng, G. Liu, J. Dai, Y. Yan, B. Zhu, R. He, L. Xie, S. Xu, X. Chen, W. Yao, X. Cui, *Sci. Rep.*, 2013, 1608.
23 W. Zhao, Z. Choranevis, K. Amara, J. Pang, M. Toh, X. Zhang, C. Kloc, P. Tan and G. Eda. *Nanoscale.*, 2013, **5**, 9677.
24 X. Xue, W. Ji, Z. Mao, H. Mao, Y. Wang, X. Wang, W. Ruan, B. Zhao and J. Lombardi. *J. Phys. Chem. C.,* 2012, **116**, 8792.
25 L. K. Pan, C. Q. Sun, C. M. Li. *J. Phys. Chem. B* 2004, **108**, 3404.
26 W. Zhao, Z. Ghorannevis, K. K. Amara, J. R. Pang, M. Toh, X. Zhang, C. Kloc, P. H. Tan, G. Eda, *Nanoscale.,* 2013, **5**, 9677.
27 C. Backes, R. J. Smith, N. McEvoy, N. C. Berner, D. McCloskey, H. C. Nerl, A. O'Neill, P. J. King, T. Higgins, D. Hanlon, *Nat. Commun.,* 2014, **5**, 5576.
28 G. Eda, H. Yamaguchi, D. Voiry, T. Fujita, M. Chen, M. Chhowalla, *Nano Lett.,* 2011, **11**, 5111.
29 W. Zhao, Z. Ghorannevis, L. Chu, M. Toh, C. Kloc, P.-H. Tan, G. Eda, *ACS Nano.,* 2013, **7**, 791.
30 B. Qu, Q. Ouyang, X. Yu, W. Luo, L. Qi, Y. *Chen., Phys. Chem. Chem Phys.,* 2015, **17**, 6036.
31 N. Dong, Y. Li, Y. Feng, S. Zhang, X. Zhang, C. Chang, J. Fan, L. Zhang, J. Wang., Sci. Rep., 2015, **5**, 14646.
32 S. Zhang, N. Dong, N. McEvoy, M. O'Brien, S. Winters, N. Berner, N. Yim, Y. Li, X. Zhang, Z. Chen, L. Zhang, G. Duesberg, J. Wang, *ACS. Nano.*, 2015, **9**, 7142.
33 Y. Li, N. Dong, S. Zhang, X. Zhang, Y. Feng, K. Wang, L. Zhang, J. Wang, *Laser Photonics Rev*., 2015, **9**, 427.
34 G. Lim, Z. Chen, J. Clark, R. G. S. Goh, W. Ng, H. Tan, R. H. Friend, P. K. H. Ho, L. Chua, *Nat. Photonics.,* 2011, **5**, 554.
35 M. Feng, R. Sun, H. Zhan, Y. Chen, *Carbon.,* 2010, **48**, 1177.
36 L. Polavarapu, N. Venkatram, W. Ji, Q.H. Xu, *ACS Appl. Mater. Inter.,* 2009, **1**, 2298.
37 L. Tao, B. Zhou, G. Bai, Y. Wang, S. F. Yu, S. P. Lau, Y. H. Tsang, J. Yao, D. Xu, *J. Phys. Chem. C.,* 2013, **117**, 23108.
38 J. Balapanuru, J.X. Yang, S. Xiao, Q. Bao, M. Jahan, L. Polavarapu, J. Wei, Q.H. Xu, K. P. Loh, *Angew. Chem. Int. Ed.,* 2010, **122**, 6699.
39 M. Feng, H. Zhan, Y. Chen, *Appl. Phys. Lett.,* 2010, **96**, 033107.
40 B. L. Li, H. L. Zou, L. Lu, Y. Yang, J. L. Lei, H. Q. Luo, and N. B. Li, *Adv. Funct. Mater.*, 2015, **25**, 3541.
41 D. Gopalakrishnan, D. Damien, M. M. Shaijumon, *ACS Nano.,* 2014, **8**, 5297.
42 R. I. Woodward, E. J. R. Kelleher, R. C. T. Howe, G. Hu, F. Torrisi, T. Hasan, S. V. Popov, J. R. Taylor. *Opt Express.*, 2014, **22**, 31113.
43 A. W. Achtstein, J. Hennig, A. Prudnikau, M. V Artemyev, U. Woggon, *J. Phys. Chem. C.,* 2013, **117**, 25756.
44 Q. Liu, B. Guo, Z. Rao, B. Zhang, J. R. Gong, *Nano Lett.,* 2013, **13**, 2436.



 